Radiative and Dynamical Feedbacks Over the Equatorial Cold-Tongue: Results from Seven Atmospheric GCMs

D.-Z. Sun and T. Zhang
Climate Diagnostics Center, NOAA-CIRES

C. Covey and S. Klein
Lawrence Livermore National Laboratory

W.Collins, J. Kiehl, and J. Meehl
National Center For Atmospheric Research

I. Held
Geophysical Fluid Dynamics Laboratory, NOAA

M. Suarez
National Aronics and Space Administration

January 26, 2005

(Submitted to J. Climate)

Abstract

The equatorial Pacific is a region with strong negative feedbacks. Yet coupled GCMs have exhibited a propensity to develop a significant SST bias in that region, suggesting an unrealistic sensitivity in the coupled models to small energy flux errors that inevitably occur in the individual model components. Could this "hypersensitivity" exhibited in a coupled model be due to an underestimate of the strength of the negative feedbacks in this region? With this suspicion, the feedbacks in the equatorial Pacific in seven atmospheric GCMs (AGCMs) have been quantified using the interannual variations in that region and compared with the corresponding calculations from the observations. The seven AGCMs are: the NCAR CAM1, the NCAR CAM2,the NCAR CAM3, the NASA/NSIPP Atmospheric Model, the Hadley Center Model (HadAM3), the GFDL AM2p10, and the GFDL AM2p12. All the corresponding coupled runs of these seven AGCMs have an excessive cold-tongue in the equatorial Pacific.

The net atmospheric feedback over the equatorial Pacific in the two GFDL models is found to be comparable to the observed value. All other models are found to have a weaker negative net feedback from the atmosphere—a weaker regulating effect on the underlying SST than the real atmosphere. A weaker negative feedback from the cloud albedo and a weaker negative feedback from the atmospheric transport are the two leading contributors to the weaker regulating effect from the model atmosphere. All models overestimate somewhat the positive feedback from water vapor. These results confirm the suspicion that an underestimate of negative feedbacks from the atmosphere over the equatorial Pacific region is a prevalent problem. The results also suggest, however, that a weaker regulatory effect from the atmosphere is unlikely solely responsible for the "hypersensitivity" in all models. The need to validate the feedbacks from the ocean transport is therefore highlighted.

1.Introduction

The equatorial Pacific is a region with strong negative feedbacks. Ramanathan and Collins (1991) first observed that a SST anomaly in the central Pacific triggers a negative response from clouds—clouds reflect more (less) solar radiation back to space in response to a positive (negative) SST changes. They even postulated that this negative feedback of cloud albedo may be a "thermostat" of the tropics. Subsequent studies point out the importance of the feedbacks from the atmospheric and oceanic dynamics (Fu et al 1990, Wallace 1992, Pierrehumert 1995, Sun and Liu 1996). In an attempt to assess the relative importance of the cloud albedo feedback and the feedback from dynamics, Sun and Trenberth (1998) used the best data available and quantified the changes in the heat transport in the atmosphere and in the ocean associated with the 1986-87 El Niño warming in addition to calculating the changes in the radiative fluxes. The results show that the negative feedback from the cloud albedo is actually a smaller player compared to the other two negative feedbacks in the equatorial Pacific region, namely the feedback from the heat transport by the atmospheric circulation and the feedback from the poleward heat transport by the ocean circulation. The negative feedback from the poleward ocean heat transport is found to be twice as strong as the negative feedback from the atmospheric transport. The latter is in turn twice as strong as the cloud albedo feedback. Against this background, the prevalence of a profound bias in the central equatorial Pacific in coupled GCMs is a surprise. To be sure, the lack of phytoplankton in the model ocean could lead to an underestimate of the solar radiation absorbed by the ocean (Murtugudde et al. 2002). The lack of sufficient vertical resolution of the ocean model may also lead to an excessive cooling of the surface ocean (Stockdale et al. 1998). The winds are not perfect in the atmospheric models and

the errors may induce excessive equatorial upwelling upon coupling. However, the fact that the excessive cold-tongue is mostly a problem of coupled models suggest that the errors in the energy and momentum fluxes in the individual components of the coupled model are small. The question that is particularly puzzling to us is that given the existence of a myriad of strong negative feedbacks, why the SST in this region, when simulated by a coupled model, appears to be sensitive to small flux errors in the model components? Could it be that the strength of one or more negative feedbacks in the model underestimated? Or alternatively, could it be that the strength of one or more positive feedbacks in the model is overestimated?

A preliminary attempt to answer these questions was made by Sun et al. (2003). By examining the response of radiative and dynamical fluxes to ENSO in the NCAR CCM3, they noted that the negative feedback of cloud albedo is substantially underestimated in the model. In further light of some coupled experiments, they put forward the hypothesis that a weaker regulating effect from the atmosphere may be a significant contributor to the development of an excessive cold-tongue in the corresponding coupled model. The purpose of this study is to extend the same analysis to six additional models whose corresponding coupled runs also have an excessive cold-tongue in the equatorial Pacific. The almost ubiquitous presence of an excessive cold-tongue in the equatorial Pacific in the coupled GCMs offers a unique opportunity to understand the causes for this syndrome: a hypothesis developed in one model can be readily tested against other models.

2. Methods

The study employs the same method of Sun et al. (2003). We use the surface warming associated

with El Niño as the forcing signal. We will then examine how radiative fluxes at the top of the atmosphere (TOA) and the vertically integrated transport of energy in the atmosphere vary in relation to the underlying SST. We quantify the feedbacks by regressing the corresponding fluxes to the SST.

The cloud and water vapor feedbacks in this paper are measured in the same way as that of Cess and Potter (1988): water vapor feedback is equated with the change in the greenhouse effect in the clear sky region, and the cloud feedbacks are equated with the corresponding changes in the long-wave and short-wave cloud forcing. These measures are not the same as the measures of Wetherald and Manabe (1988) which use offline radiative transfer calculations to obtain the true partial derivatives (Soden et al. 2004). The measures of Cess and Potter (1988) tend to overestimate the feedback from the greenhouse effect of water vapor and underestimate the feedback from the greenhouse effect of clouds. However, provided the feedbacks in the models are measured in the same way as in the observations, the errors revealed in the analysis are still true errors in the models. The available radiation data measure the feedbacks of water vapor and clouds on the ENSO time-scale in the form of Cess and Potter (1988). Also, the concern here is more with the combined effect of water vapor and cloud feedbacks on the response in the net surface heat flux into the ocean—the net atmospheric feedback—than with the accuracy in the definition of individual feedbacks of water vapor and clouds, the distinctions between the measures of Cess and Potter (1988) and Wetherald and Manabe (1988) of the individual feedbacks of water vapor and clouds are considered less important.

The observational data comes from ERBE (Barkstrom et al. 1989) and the NCEP reanalysis

(Trenberth et al. 2001). The model data are from the AMIP runs over the ERBE period. The AMIP runs have the observed, time-varying SST as the boundary conditions. Therefore, the model atmosphere is subject to the same SST forcing as the real atmosphere.

The models that have been analyzed are the models that have a corresponding coupled run without the use of flux adjustment. These models are (1) the NCAR CAM1 (Kiehl et al. 1998), (2) the NCAR CAM2 (Collins et al. 2003), (3) the NCAR CAM3 (Collins et al. 2004), (4) the NASA NSIPP model (Chou and Suarez 1996, Suarez 1995), (5) the Hadley Center Model (Collins et al. 2001), (6) the GFDL AM2p10, and (7) the GFDL AM2p12 (The GFDL Global Atmospheric Model Development Team, 2004). (The GFDL AM2p10 is an earlier version of the GFDL AM2p12. The main differences between the two versions are in the use of boundary layer schemes and in the vertical layers. The AM2p10 uses the boundary layer scheme of Mellor and Yamada (1974) while the AM2p12 uses the boundary layer scheme of Lock et al. (2000). The AM2p12 has 24 vertical layers while the AM2p10 has 18 vertical layers).

The seven models involve the use of four different schemes for most convection. The NCAR models use the deep convection scheme by Zhang and McFarlane (1995) and the shallow convection scheme by Hack (1994). The NASA NSIPP model and the two GFDL models use the Relaxed Arakawa Schubert (RAS) scheme (Moorthi and Suarez 1992). The Hadley Center model uses a mass-flux scheme (Gregory 1990, Gregory and Rowntree 1990) that is based on the bulk cloud model of Yanai et al. (1973). The seven models also have different vertical and horizontal resolutions. The vertical resolutions vary from 18 layers (NCAR CAM1) to 34 layers (NASA NSIPP). The horizontal resolutions vary from about 3.8^{o}X2.5^{o} in the Hadley Centre

model to 2.5°X2.0° in the GFDL and the NASA models. Despite the many differences in these seven atmosphere models, gauged by the meridional and zonal SST gradients over the equatorial Pacific, all their corresponding coupled models have an excessive cold-tongue over the central equatorial Pacific (Fig. 1).

3. Results

The estimates of the feedbacks from these models over the central equatorial Pacific region (150°E-250°E, 5°S-5°N) are summarized in Table 1. The definition of the symbols and the procedure of the calculations are the same as in Sun et al. (2003). $\frac{\partial}{\partial T}G_a$ is the water vapor feedback, $\frac{\partial}{\partial T}C_l$ is the feedback from the greenhouse effect of clouds, $\frac{\partial}{\partial T}C_s$ is the feedback from the short-wave forcing of clouds, and $\frac{\partial}{\partial T}D_a$ is the feedback from the atmospheric transport. $\frac{\partial F_a}{\partial T} = \frac{\partial G_a}{\partial T} + \frac{\partial C_l}{\partial T} + \frac{\partial C_s}{\partial T} + \frac{\partial D_a}{\partial T}$ and is termed as the net atmospheric feedback. $\frac{\partial}{\partial T}F_s$ is the feedback from net surface heat flux into the ocean. Neglecting the heat storage in the atmosphere, which is small (Sun 2000), $\frac{\partial}{\partial T}F_s$ differs $\frac{\partial}{\partial T}F_a$ by a constant—the rate of change of the ocean's surface emission with respect to SST.

With the exception of the two GFDL models, all other models underestimate the negative feedback from the cloud albedo and the negative feedback from the atmospheric transport. The underestimate in the cloud albedo appears to be particularly worrisome as this feedback in one of these models has the opposite sign of the observed. The NCAR CAM2 differs from the observed value in its simulation of the cloud albedo feedback by as much as 12.8 W/m^2/K. With the

exception of the two GFDL models, the underestimate of the strength of the negative feedback from the atmospheric transport in these models are also significant. The error ranges from 4.6 $W/m^2/K$ in the Hadley Center model to 7.7 $W/m^2/K$ in the NCAR CAM3. All models overestimate the positive feedback from water vapor. The error ranges from 15%--50%. The GFDL AM2p10 has the smallest error in the simulation of the water vapor feedback while the largest error is found in the Hadley Center model. Models also err on the estimate of the feedback from the long-wave forcing of clouds, but they do not bias toward the same direction. While the NCAR CCM3 (CAM1) overestimates the feedback from the long-wave forcing of clouds by 3.7 $W/m^2/K$, the NCAR CAM2 underestimates this feedback by 5.6 $W/m^2/K$. The underestimate of the feedback from the long-wave forcing of clouds in the Hadley Centre model is also large (4.6 $W/m^2/K$). The underestimate of the positive feedback from the long-wave forcing of clouds in the NCAR CAM2, the NCAR CAM3, the NASA NSIPP model, and the Hadley Centre model alleviates the effect of the errors on the net atmospheric feedback from the underestimate of the cloud albedo feedback and the overestimate of the water vapor feedback.

Because of the underestimate of the negative feedbacks from the cloud short-wave forcing and the atmospheric transport and to a less degree because of the overestimate of the positive feedback from water vapor, the negative net atmospheric feedback in all other models except the two GFDL models is underestimated over the region of concern. The results confirm the suspicion that underestimating the strength of the negative feedbacks in the region of concern is a prevalent problem in the climate models. The results from the GFDL models, however, are very encouraging. The net atmospheric feedback in the two GFDL models is comparable to the observed value. The improvements in the GFDL models are not just from the improvements in

the cloud albedo feedback, but from the improvements in the feedback from the atmospheric transport.

The horizontal pattern of the response in G_a to ENSO forcing from the models show remarkable agreement with each other and with observations. Within the region of concern, the response of G_a in the models is greater than in the real world grid-point by grid-point (Fig. 2). It is therefore tempting to suggest that the overestimate of $\frac{\partial}{\partial T}G_a$ in the equatorial Pacific in the models is because these models are still too diffusive in the vertical (Sun and Held 1996). It is interesting to note, however, that the AM2p12 overestimates $\frac{\partial}{\partial T}G_a$ more than the AM2p10 does even though the latter is a version that has fewer vertical levels. The increased levels in the AM2p12 are all in the boundary layer and one may still hope that increased vertical resolution throughout the troposphere can make a difference, but Ingram (2002) examined a wide array of GCMs and also noted that the increases in the vertical resolution in the models do not result in a weaker water vapor feedback. Four different cumulus parameterization schemes are used in the models analyzed here. The overestimate of the water vapor feedback in all models is thus particularly puzzling. One thing that all the four parameterization schemes lack is the inclusion of the effect of sub-grid scale variability. Whether the neglect of the effect of sub-grid scale variability makes the model atmosphere appear to be more "diffusive" emerges as a question of interest. The difference in the value of $\frac{\partial}{\partial T}G_a$ between the two versions of the GFDL model raises another question of potential interest: why the water vapor feedback in the model appears to be sensitive to the use of different boundary layer schemes?

While the spatial patterns of the response of G_a, in different models are strikingly similar, there is more variability in the response of C_l (Fig.3). The NASA model is particularly notable--the response of C_l in the equatorial central Pacific near the dateline (180^oE-140^oW) is much weaker than the observed (Fig. 3e). This equatorial minimum response splits the response of C_l to El Nino warming into two parts, each of which has a maximum off the equator. The response of C_s and the rainfall in the NASA NSIPP model also has this "split pea" feature (Fig.4e and Fig.5e), indicating a lack of response of convection in the central equatorial Pacific near the date line in the model. The lack of response of D_a in the same region in the NASA model (Fig. 6e) also suggests a lack of response of convection in the central equatorial Pacific.

Contrasting the spatial patterns in the response of the cloud forcing (Fig.3 and Fig.4) with the spatial patterns in the rainfall (Fig.5) confirms the impression that the leading source of errors in the response of C_s may still be the most obvious: errors in the response of convection. The rainfall responses in the equatorial central Pacific in the CAM2 and the CAM3 are the two weakest, so are their responses in C_s. The improvement in the response in C_s in the HadAM3 and the GFDL models apparently follows the improvement in the response of convection. All models predict a maximum precipitation response over the equatorial region near the dateline, but the GFDL models have the strongest responses in this region.

The response of convection in the model does not have the same control over the response of C_l as over the response of C_s: the HadAM3 has a response in rainfall that is comparable to observations, but the response in C_l in the same model is only half of the value from observations. Convection also has a lesser control over the response in G_a. For example, the

rainfall in the NCAR CAM2 and CAM3 is much weaker than that in CAM1, but the response in G_a in the NCAR CAM2 and CAM3 is only slightly weaker than that in CAM1.

The three NCAR models and the NASA model are the models that have a poor simulation of the response in D_a. The cause of their poor simulation of the response of D_a is apparently the same as the cause of their poor simulation of the response of C_s: the lack of response of convection on the equator near the date line region. The maximum response of precipitation response is located off equator in these four models. The NCAR models do not appear to be a distinct lack of response in precipitation over the central equatorial Pacific where there is a distinct lack of response in D_a. However, the responses in the precipitation in the NCAR CAM2 and the NCAR CAM3, are weak throughout the concerned region (Fig. 5c, d).

The impact of the errors in the aforementioned feedbacks on the response of the net surface heating (F_s) is further shown in Fig. 7, which gives a basin-wide, and a more critical view of the response of the model atmosphere. In four of the seven models (the NCAR CAM1, CAM2, CAM3, and the NASA NSIPP, the response of the surface heating to El Nino warming in the equatorial central Pacific (160^{o}E-140^{o}W) has the wrong sign. The response of F_s in the Hadley Center model in the same region is near zero. The two GFDL models have adequate responses in the equatorial central Pacific. One of them—the GFDL AM2p10-- suffers a significant deficiency in the region east to about 120^{o}W. The negative response in the GFDL AM2p10 also does not extend as far west as in the observations. The zonal extent of the response in the later version of the GFDL model—the AM2p12—is improved, but the meridional extend of the

response is more confined. Still, the spatial pattern of the response of F_s in both the GFDL models resembles the observed remarkably well.

Diagnosing the root causes of all the model deficiencies is beyond the scope of the present paper and may require more sophisticated tools than simple regression analysis here. The encouraging part of the present analysis is that it may not be a difficult task to have all the feedbacks right: the GFDL AM2p10 provides an example. Whether this good agreement between the simulations by the GFDL model and the observations is simply a matter of luck or truly reflecting the fidelity of the model to Nature needs to be further examined.

4. Discussion

The results from this analysis highlight that it remains a difficult issue to simulate the cloud and water vapor feedbacks over the equatorial Pacific by GCMs. Consistent with earlier analyses, the errors in the cloud feedbacks are most prominent. Most models tend to underestimate the strength of the negative feedback from cloud albedo. The errors in the water vapor feedback are also significant and call for renewed attention to the issue of water vapor feedback. Soden (1997) suggested a more optimistic picture about the accuracy of water vapor feedback in GCMs, but his analysis is focused on the response of the tropical mean greenhouse effect of water vapor to El Nino warming, and is limited to a single GCM—the GFDL R-15 model (Wetherald et al. 1991).

While the analysis has revealed some common deficiencies in the simulation of atmospheric feedbacks by GCMs, the results also suggest that the common errors in the atmospheric feedbacks are unlikely the sole cause of the excessive cold-tongue in the central equatorial Pacific. The simulation of the atmospheric feedbacks in the GFDL AM2p10 is probably as close to the observed as one can reasonably hope, but the corresponding coupled model still has an excessive cold-tongue (Fig. 1g). The results highlight the need to look at the ocean feedbacks. One way to do so is to check the response of the surface wind stress to changes in the SST and then the response of the ocean heat transport to the changes in the wind stress. The former can be assessed to some degree using the AMIP runs of the atmospheric GCMs. The obstacle for carrying out this analysis immediately is the lack of good data for the tropical wind stress. The limited satellite data (Liu 2002) has revealed severe deficiencies in the NCEP reanalysis, but the satellite data are still too short for calculating feedbacks. The latter requires forced ocean experiments from different groups using the same surface forcing. These forced ocean model experiments are not yet available on the scale of the AMIP experiments. Nor is it clear whether the accuracy of ocean heat transport data is sufficient to validate the results from the model experiments.

The present analysis has a linear perspective built in, and therefore the results are more relevant for the initial development of the excessive cold-tongue. After a significant cold SST bias in the central equatorial Pacific develops in the modeled climate, it may displace the convection so far west that the associated atmospheric feedbacks cease operating in the central equatorial Pacific. The study by Wittenberg et al. 2004 suggests that GFDL models may have this nonlinear effect. Other models probably have this nonlinear effect too. Nonetheless, it is logical to first identify

the factors that are responsible for the initial growth of the excessive cold-tongue and then examine how excessive cold-tongue in the coupled model maintains its stability. This consideration of priorities points a direction to extend the present study, which is to use directly the outputs from coupled models to quantify the feedbacks in the cold-tongue region. The drawback of using the ENSO signals in the coupled models is that the signals are not the same as in the real world, but the results may shed light on the question how the excessive cold-tongue in the coupled model maintains its stability.

Underestimating the negative feedbacks in the central equatorial Pacific does not suggest that the models overestimate global warming. The forcing due to increases in CO_2 is not the same as the El Niño warming. Nonetheless, our confidence with the model predictions of global warming may have to come from how well the model simulate the feedbacks on the shorter time-scales because it is over these time-scales we have better data and know more quantitatively the feedbacks in Nature.

.

References:

Barkstrom, B.R., E.F. Harrison, G.L. Smith, R. Green, J. Kibler, R.D. Cess, and the ERBE Science Team, 1989: Earth Radiation Budget Experiment (ERBE) Archive and April 1985 Results. *Bull. Amer. Meteror. Soc.,* 70, 1254-1262.

Boville, B. A., and P. R. Gent, 1998: The NCAR Climate System Model, Version One. J. Climate, 11, 1115-1130.

Cess, R. D., and G. L. Potter, 1988: A methodology for understanding and intercomparing atmospheric climate feedback processes in general circulation models. J. Geophys. Res., 93, 8305–8314.

Chou, M.-D., and M.J. Suarez, 1996: A Solar Radiation Parameterization (CLIRAD-SW). NASA Technical Memorandum no. 104606, v. 15, 48 pp.

Collins, W. D., J. J. Hack, B. A. Boville, P. J. Rasch, D. L. Williamson, J. T. Kiehl, B. Briegleb, J. R. McCaa, C. Bitz, S.-J. Lin, R. B. Rood, M. Zhang, and Y. Dai, 2003: Description of the NCAR Community Atmosphere Model (CAM2). 171pp. [Available online at http://www.ccsm.ucar.edu/models/atm-cam/docs/cam2.0/description.pdf.]

Collins, W. D., P. J. Rasch, B. A. Boville, J. J. Hack, J. R. McCaa, D. L. Williamson, J. T. Kiehl, B. Briegleb, C. Bitz, S.-J. Lin, M. Zhang, and Y. Dai, 2004: Description of the NCAR Community Atmosphere Model (CAM 3.0), Technical Report NCAR/TN-464+STR, National Center for Atmospheric Research, Boulder, Colorado, 210 pp.

Collins, M., S.F.B. Tett, and C. Cooper, 2001: The internal climate variability of a HadCM3, a version of the Hadley Centre coupled model without flux adjustments. *Clim. Dyn.,* 17: 61-81.

Delworth, T. L., et al., 2004: GFDL's CM2 global coupled climate models - Part I: Formulation and simulation characteristics. J. Clim. (submitted)

Fu, R., DelGenio, A.D., Rossow, W.B., and Liu, W.T., 1990: Cirrus cloud thermostat for tropical sea surface temperature tested using satellite data. *Nature*, 358, 394-397.

Gregory, D., 1990: Convection scheme. Unified Model Documentation Paper No. 27, United Kingdom Meteorological Office, Bracknell, Berkshire RG122SZ, UK.

Gregory, D., and P.R.R. Rowntree, 1990: A mass flux convection scheme with representation of cloud ensemble characteristics and stability dependent closure. Mon. Wea. Rev., 118, 1483-1506.

Hack, J. J., 1994: Parameterization of moist convection in the National Center for Atmospheric Research Community Climate Model (CCM2). *J. Geophys. Res.,* **99**, 5551-5568.

Ingram, W.J., 2002: On the Robustness of the Water Vapor Feedback: GCM Vertical Resolution and Formulation. *J. Climate*, 11, 1131-1149.

Kiehl, J., J. J. Hack, G. Bonan, B. A. Boville, D. Williamson, and P. J. Rasch, 1998: The National Center for Atmospheric Research Community Climate Model: CCM3. *J. Climate*, 11, 1131-1149.

Kiehl, J. T., and P. R. Gent, 2004: The Community Climate System Model, Version Two. J. Clim., 17, 3666-3682.

Liu, W. T., 2002: Progress in scatterometer applications. *J. Oceanogr*., 58, 121–136.

Lock, A. P., A. R. Brown, M. R. Bush, G. M. Martin, and R. N. B. Smith, 2000: A new boundary layer mixing scheme. Part I: Scheme description and single-column model tests. Mon. Wea. Rev., 128, 3187-3199.

Mellor, G.L., and T. Yamada, 1974: A hierarchy of turbulence closure models for planetary boundary layers, *J. Atmos. Sci*. ,**31**, 1791-1806.

Moorthi, S. and M. Suarez, 1992: Relaxed Arakawa-Schubert: a parameterization of moist

convection for general circulation models. Mon. Wea. Rev., 120, 978-1002.

Murtugudde, R., J. Beauchamp, C. R. McClain, and A. J. Busalacchi, 2002: Effects of penetrative radiation on the upper tropical ocean circulation. *J. Climate*, 15, 470-496.

Pierrehumbert, R. T., 1995: Thermostats, radiator Fins, and the local runaway greenhouse. *J. Atmos. Sci.,* 52, 1784-1806.

Ramanathan, V. and W. Collins, 1991: Thermodynamic regulation of ocean warming by cirrus clouds deduced from observations of the 1987 El Niño. *Nature*, 351, 27-32.

Rayner, N. A., Horton E. B., Parker D. E., Folland C. K., and Hackett R. B., 1996: Version 2.2 of the global sea-ice and sea surface temperature data set, 19031994. Climate Research Tech. Note 74 (CRTN74), Hadley Centre for Climate Prediction and Research, Met Office, United Kingdom, 35 pp.

Soden, B., 1997: Variations in the tropical Greenhouse effect during El Nino. *J. Climate*, **10**, 1050-1054.

Soden, B., A.J. Broccoli, and R.S. Hemler, 2004: On the Use of Cloud Forcing to Estimate Cloud Feedbacks. *J. Climate*, **17**, 185-205.

Stockdale, T.N., A.J. Busalacchi, D.E. Harrison, and Richard Seager, 1998: Ocean Modeling for ENSO. *J. Geophys. Res.,* 103, 14,325-14,355.

Suarez, M.J., 1995: Documentation of the ARIES/GEOS Dynamical Core, version 2. NASA Technical Memorandum no. 104606, v. 5, 53 pp

Sun, D.-Z., 2000: The heat sinks and sources of the 1986-87 El Niño. *J. Climate*, **13**, 3533-3550.

Sun, D.-Z., and I. Held, 1996: A comparison of modeled and observed relationships between interannual variations of water vapor and temperature. *J. Climate*, **9**, 665-675.

Sun, D.-Z. and Z. Liu, 1996: Dynamic ocean-atmosphere coupling: a thermostat for the tropics.

Science, 272, 1148-1150.

Sun, D.-Z., J. Fasullo, T. Zhang, and A. Roubicek, 2003: On the radiative and dynamical feedbacks over the equatorial Pacific cold-tongue. *J. Climate.*, **16,** 2425—2432.

Sun. D.-Z. and K. E. Trenberth, 1998: Coordinated heat removal from the tropical Pacific region during the 1986-87 El Niño. *Geophys. Res. Lett.,* 25, 2659-2662.

The GFDL Global Atmospheric Model Development Team, 2004: The new GFDL global atmosphere and land model AM2/LM2: Evaluation with prescribed SST simulations. *J. Climate*, **17,** 4641-4673.

Trenberth, K.E., J.M. Caron, and D.P. Stepaniak, 2001: The atmospheric energy budget and implications for surface fluxes and ocean heat transport. *Climate Dyn*., **17**, 259-296.

Wallace, J.M., 1992: Effect of deep convection on the regulation of tropical sea surface temperature. *Nature*, 357, 230-231

Wetherald, R. T., and S. Manabe, 1988: Cloud feedback processes in a general circulation model. J. Atmos. Sci., 45, 1397–1415.

Wetherald, R. T., V. Ramaswamy, and S. Manabe, 1991: A comparative study of the observations of high clouds and simulations by an atmospheric general circulation model. Climate Dyn., 5, 135–143.

Wittenberg, A.T., A. Rosati, N.-C. Lau, and J. J. Ploshay, 2004: GFDL's CM2 Global Coupled Models, Part 3: Tropical Pacific Climate and ENSO. *J. Climate,* Submitted.

Xie, P., and P.A. Arkin, 1996: Analyses of Global Monthly Precipitation Using Gauge Observations, Satellite Estimates, and Numerical Model Predictions. *J. Climate,* **9**, 840-858.

Yanai, M., S. Esbensen, and J.-H., Chu, 1973: Determination of bulk properties of tropical cloud clusters from large-scale heat and moisture budgets. J. Atmos. Sci., 30, 611-627.

Zhang, G.J., and N. A. McFarlane, 1995: Sensitivity of climate simulations to the parameterization of cumulus convection in the Canadian Climate Centre general circulation model. *Atmos.-Ocean*, **33**, 407-446.

Acknowledgments

This research was supported partially by NOAA's office of global programs (the Climate Dynamics Program and Experimental Prediction Program, and the CLIVAR Pacific Program), and partially by the NSF Climate Dynamics Program (ATM-9912434 and ATM-0331760). Using data from the Atmospheric Model Intercomparison Project (AMIP), this work was also partially supported under the auspices of the U.S. Dept. of Energy, Office of Science, at the University of California Lawrence Livermore National Laboratory under Contract W-7405-Eng-48. The National Center for Atmospheric Research (NCAR) is sponsored by the National Science Foundation. The leading author (D.-Z. Sun) would like to thank Dr. Robert Dickinson for his encouraging comments. D.-Z. Sun would also like to thank Dr. Ping Chang and Dr. R. Saravanan for the conversations on the causes of the double ITCZ in coupled models.

Table Legends

Table 1: Atmospheric feedbacks over the equatorial Pacific (5ºS-5ºN, 150ºE-250ºE) from seven climate models. See text for the definition of the symbols for the various feedbacks. The values for these feedbacks are obtained through a linear regression using the interannual variations of the SST and the corresponding fluxes over the equatorial Pacific.

Figure Legends

Figure 1: Tropical Pacific SST from observations (Rayner et al. 1996) and seven coupled climate models: NCAR CCSM1 (Boville and Gent 1998), the NCAR CCSM2 (Kiehl and Gent 2004), the NCAR CCSM3 (www.ccsm.ucar.edu/experiments/ccsm3.0/), the HadCM3 (Collins et al. 2001), the NASA CGCM ((http://nsipp.gsfc.nasa.gov/data_req/coupled/coupl_data_main.htl), and the two latest versions of the coupled models from GFDL (Delworth et al. 2004, http://data1.gfdl.noaa.gov/nomads/forms/decen/CM2.X/). The atmospheric components of the seven coupled models are respectively the NCAR CAM1, the NCAR CAM2, the NCAR CAM3, the NASA NSIPP GCM, the Hadely Centre model HadAM3, the GFDL AM2p10, and the GFDL AM2p12. Shown are annual mean conditions.

Figure 2: Response of the greenhoue effect of water vapor (G_a) to El Niño warming. Shown are coefficents obtained by linearly regressing the greenhouse effect of water vapor at each grid point on the SST averaged over the equatorial Pacific (5^oS-5^oN, 150^oE-250^oE). The interannual variations of G_a over the ERBE period are used for the calculations.

Figure 3: Response of the greenhouse effect of clouds (C_l) to El Niño warming. Shown are coefficents obtained by linearly regressing the greenhouse effect of clouds at each grid point on the SST averaged over the equatorial Pacific (5^oS-5^oN, 150^oE-250^oE). The interannual variations of the concerned quantities over the ERBE period are used for the calculations.

Figure 4: Response of the shortwave forcing of clouds (C_s) to El Niño warming. Shown are coefficents obtained by linearly regressing the short-wave forcing of clouds at each grid point on the SST averaged over the equatorial Pacific (5^oS-5^oN, 150^oE-250^oE). The interannual variations of the concerned quantities over the ERBE period are used for the calculations.

Figure 5: Response of the precipitation to El Niño warming. Shown are coefficents obtained by linearly regressing the precipitation at each grid point on the SST averaged over the equatorial Pacific (5^oS-5^oN, 150^oE-250^oE). The interannual variations of the concerned quantities over the ERBE period are used for the calculations. The precipitation data are from Xie and Arkin (1996).

Figure 6: Response of the convergence of vertically integrated transport of energy by the atmospheric circulations (D_a) to El Niño warming. Shown are coefficents obtained by linearly regressing the value of D_a at each grid point on the SST averaged over the equatorial Pacific (5^oS-5^oN, 150^oE-250^oE). The interannual variations of the concerned quantities over the ERBE period are used for the calculations.

Figure 7: Response of the net surface heating (F_s) to El Niño warming. Shown are coefficents obtained by linearly regressing the net surface heating at each grid point on the SST averaged over the equatorial Pacific (5^oS-5^oN, 150^oE-250^oE). The interannual variations of the concerned quantities over the ERBE period are used for the calculations. The data used for Fs are the same as in Sun et al. (2003).

Table 1

Atmospheric Feedbacks in Models and Observations

Name of Process	Feedback ($Wm^{-2}K^{-1}$)							
	Observation	NCAR/CAM1	NCAR/CAM2	NCAR/CAM3	NASA/NSIPP-1	UKMO/HadAM3	GFDL/AM2p10	GFDL/AM2p12
$\frac{\partial(G_\alpha)}{\partial T}$	6.72 ± 0.27	9.10 ± 0.43	8.39 ± 0.41	8.89 ± 0.39	8.21 ± 0.33	10.10 ± 0.48	8.08 ± 0.33	9.43 ± 0.32
$\frac{\partial(C_L)}{\partial T}$	12.21 ± 1.03	15.94 ± 1.35	6.64 ± 0.63	7.21 ± 0.72	9.14 ± 0.72	7.63 ± 0.86	13.52 ± 0.78	14.74 ± 0.96
$\frac{\partial(C_S)}{\partial T}$	-10.93 ± 1.37	-4.98 ± 0.60	1.87 ± 0.96	-0.56 ± 0.78	-5.95 ± 0.77	-8.94 ± 1.33	-12.74 ± 0.79	-12.58 ± 1.09
$\frac{\partial(D_\alpha)}{\partial T}$	-16.69 ± 1.51	-13.63 ± 1.76	-9.18 ± 1.40	-9.02 ± 1.20	-14.08 ± 0.96	-12.11 ± 1.53	-17.63 ± 0.92	-19.40 ± 1.28
$\frac{\partial(F_A)^*}{\partial T}$	-8.69 ± 1.76	6.42 ± 1.24	7.72 ± 1.12	6.53 ± 1.00	-2.69 ± 0.97	-3.33 ± 1.64	-8.77 ± 1.12	-7.81 ± 1.53
$\frac{\partial(F_S)}{\partial T}$	-14.89 ± 1.83	0.44 ± 1.24	1.48 ± 1.13	0.30 ± 1.02	-8.71 ± 0.98	-9.15 ± 1.64	-14.73 ± 1.13	-13.80 ± 1.53

The net atmospheric feedback $\frac{\partial(F_A)}{\partial T} = \frac{\partial(G_\alpha)}{\partial T} + \frac{\partial(C_L)}{\partial T} + \frac{\partial(C_S)}{\partial T} + \frac{\partial(D_\alpha)}{\partial T}$

Table 1

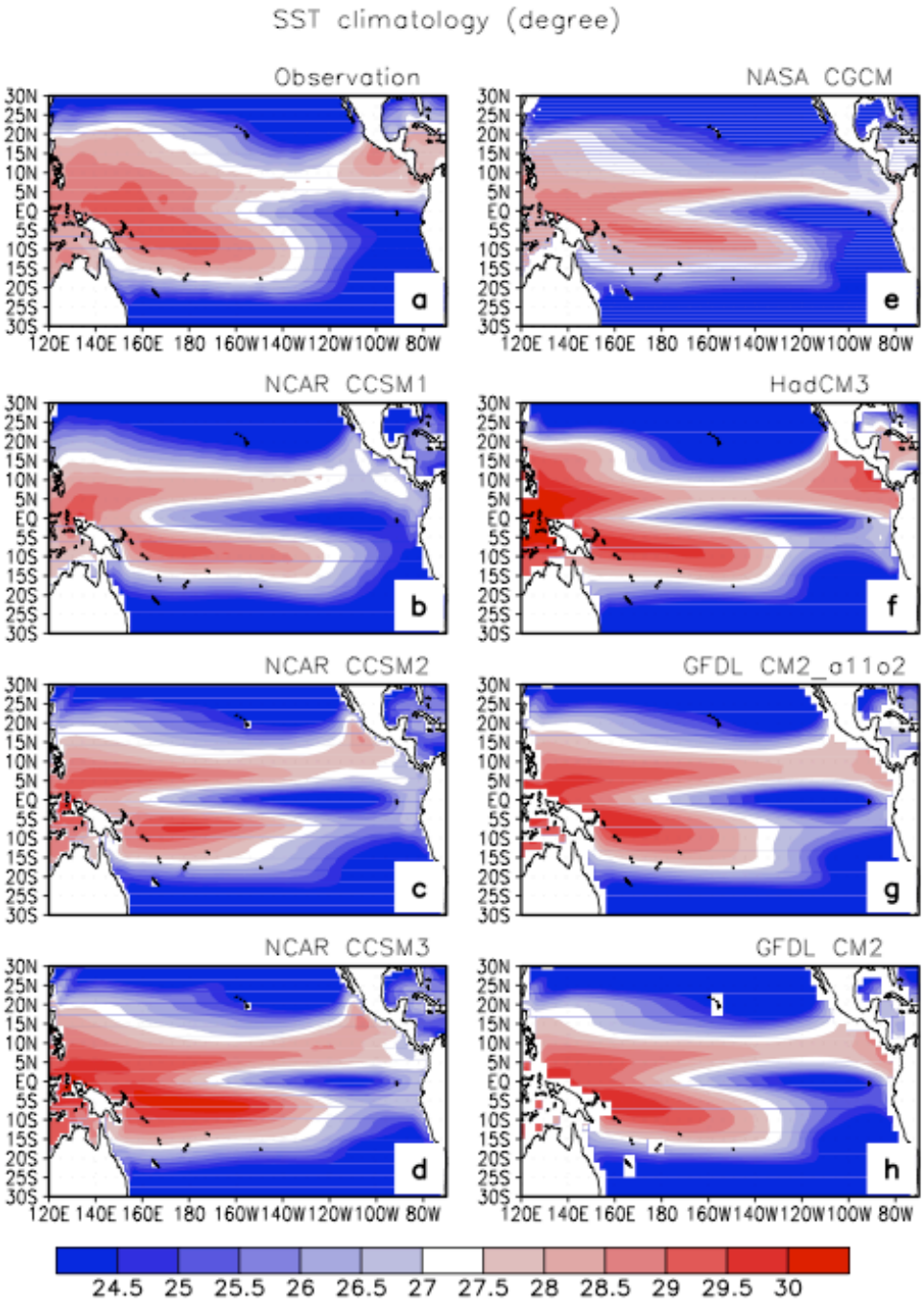
SST climatology (degree)
Observation
NASA CGCM
NCAR CCSM1
HadCM3
NCAR CCSM2
GFDL CM2_a11o2
NCAR CCSM3
GFDL CM2
a
b
c
d
e
f
g
h
30N 25N 20N 15N 10N 5N EQ 5S 10S 15S 20S 25S 30S
120E 140E 160E 180 160W 140W 120W 100W 80W
24.5 25 25.5 26 26.5 27 27.5 28 28.5 29 29.5 30

Fig.1

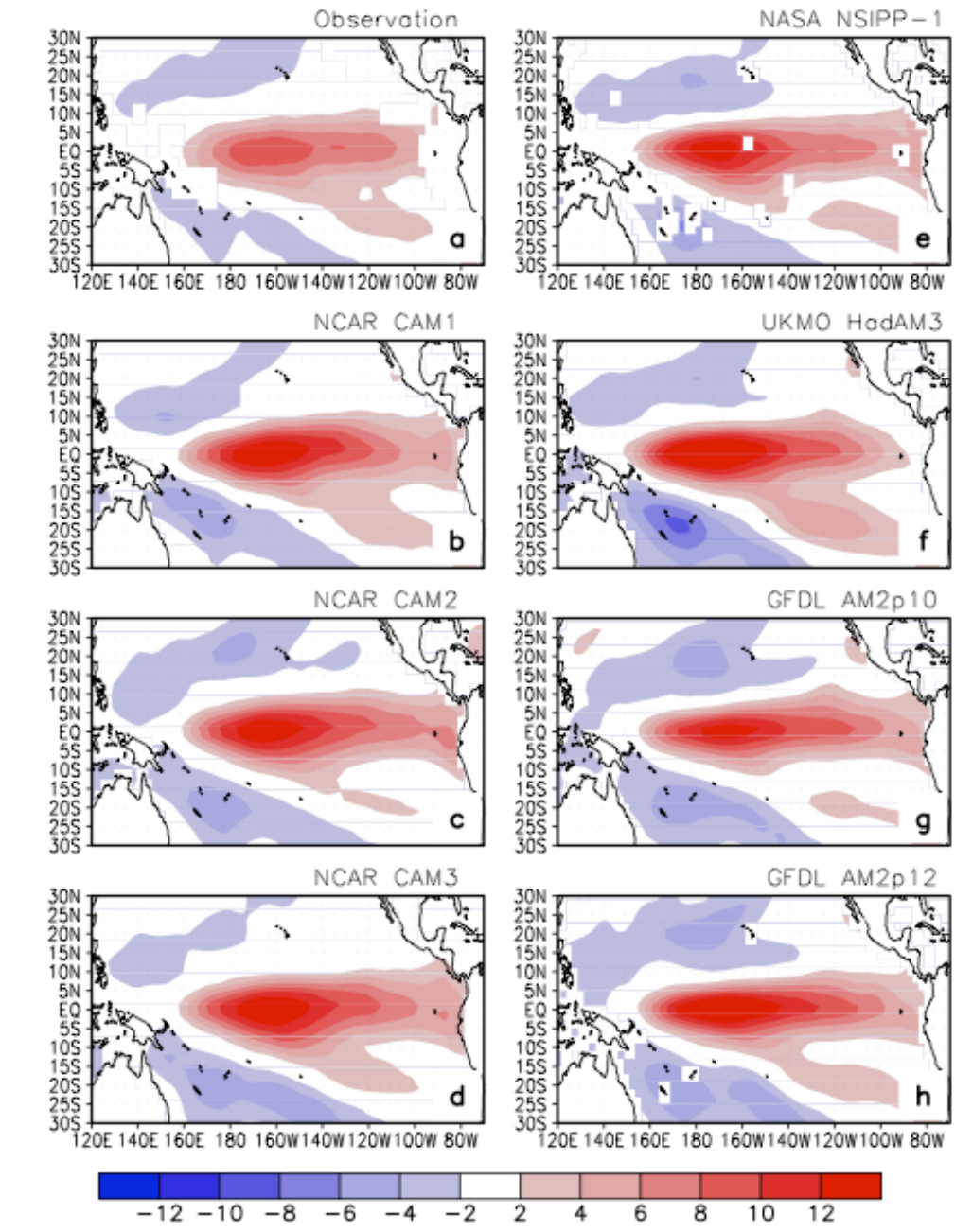
Spatial pattern of response of Ga to El Nino Warming (W/m**2/K)
Observation
NASA NSIPP-1
NCAR CAM1
UKMO HadAM3
NCAR CAM2
GFDL AM2p10
NCAR CAM3
GFDL AM2p12
30N 25N 20N 15N 10N 5N EQ 5S 10S 15S 20S 25S 30S
120E 140E 160E 180 160W 140W 120W 100W 80W
a
b
c
d
e
f
g
h
−12 −10 −8 −6 −4 −2 2 4 6 8 10 12

Fig.2

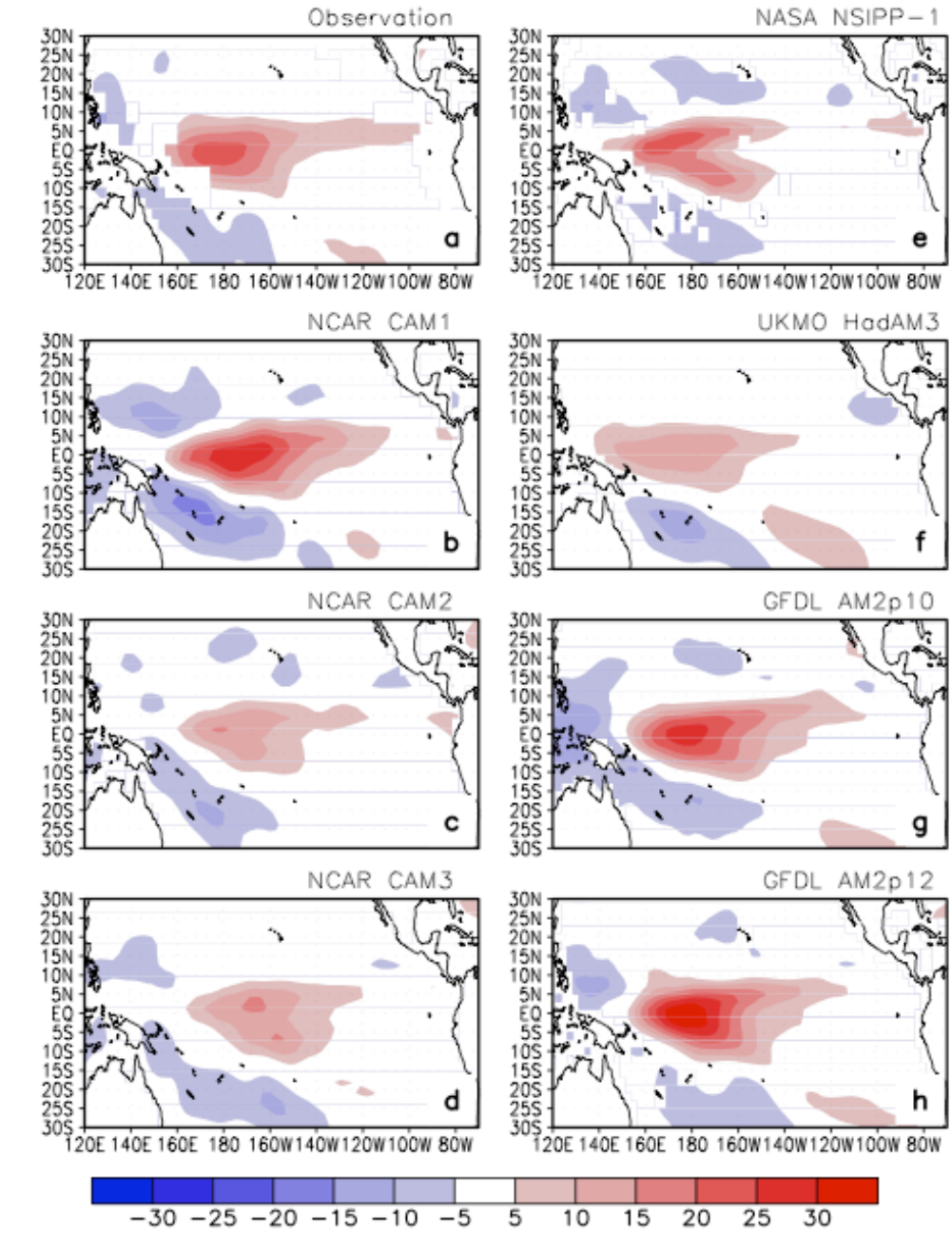
Spatial pattern of response of CI to EI Nino Warming (W/m**2/K)
Observation
NASA NSIPP-1
NCAR CAM1
UKMO HadAM3
NCAR CAM2
GFDL AM2p10
NCAR CAM3
GFDL AM2p12
a
b
c
d
e
f
g
h
30N 25N 20N 15N 10N 5N EQ 5S 10S 15S 20S 25S 30S
120E 140E 160E 180 160W 140W 120W 100W 80W
-30 -25 -20 -15 -10 -5 5 10 15 20 25 30

Fig.3

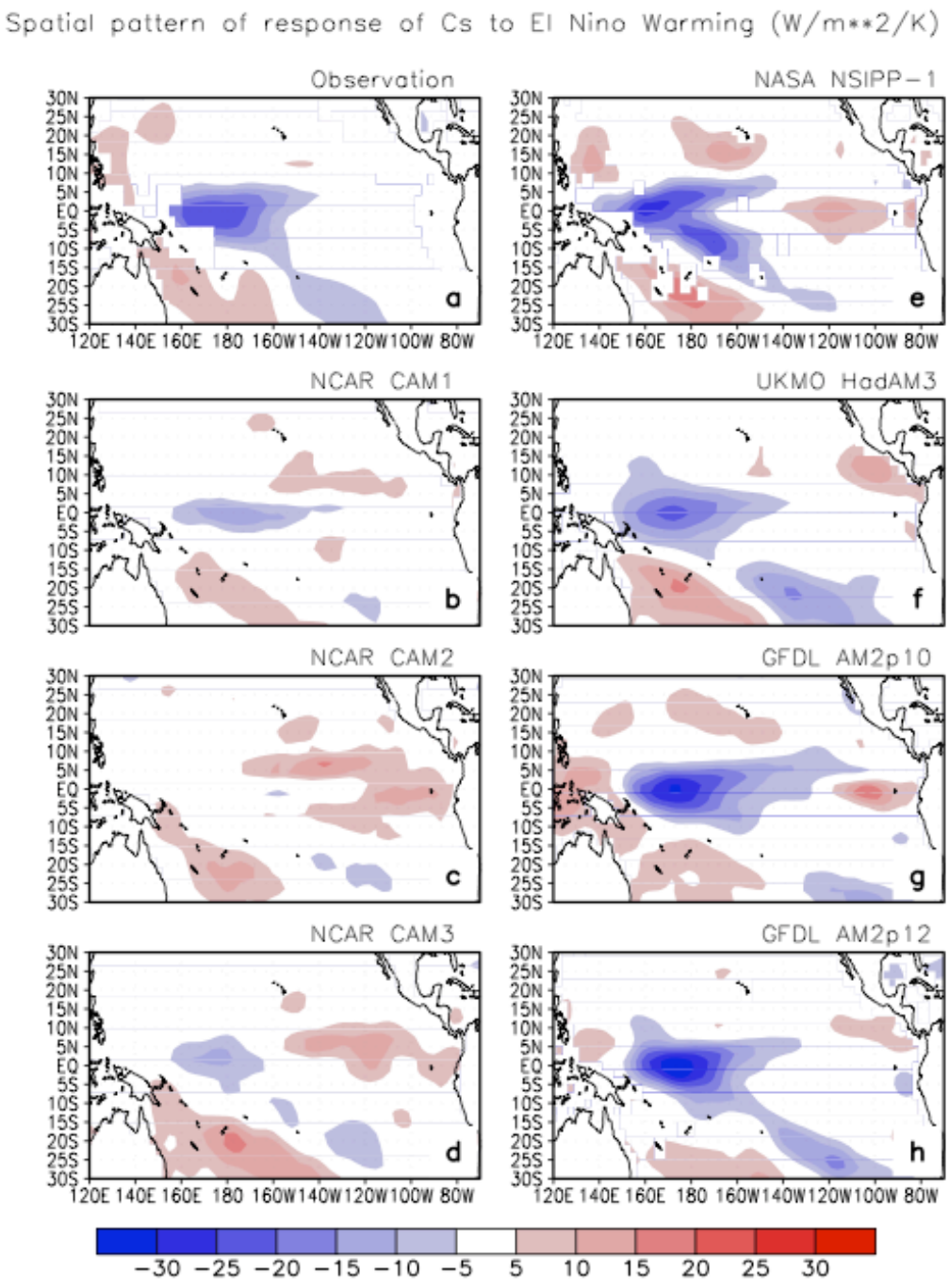
Spatial pattern of response of Cs to El Nino Warming (W/m**2/K)
Observation
NASA NSIPP-1
NCAR CAM1
UKMO HadAM3
NCAR CAM2
GFDL AM2p10
NCAR CAM3
GFDL AM2p12
a
b
c
d
e
f
g
h
30N 25N 20N 15N 10N 5N EQ 5S 10S 15S 20S 25S 30S
120E 140E 160E 180 160W 140W 120W 100W 80W
-30 -25 -20 -15 -10 -5 5 10 15 20 25 30

Fig.4

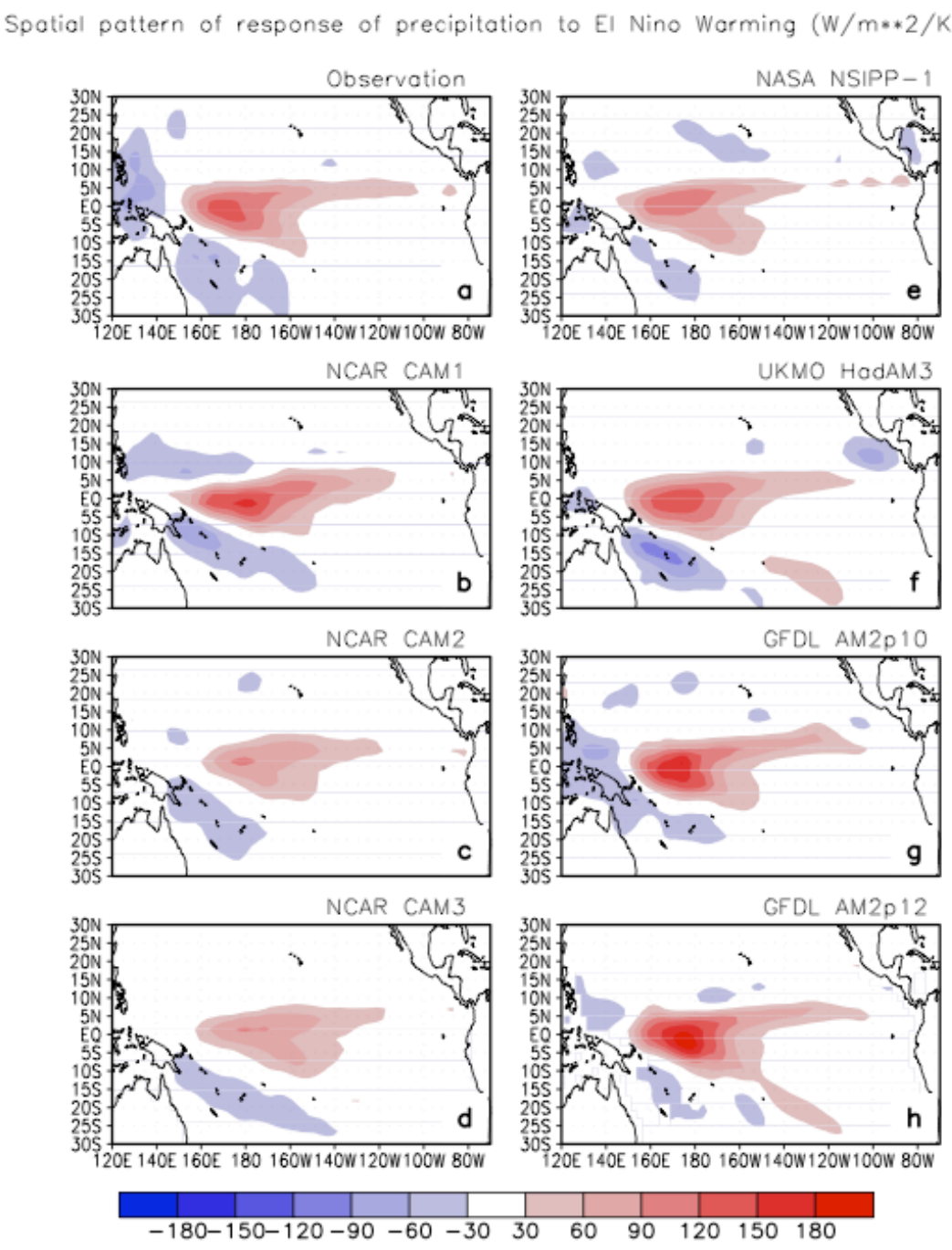
Spatial pattern of response of precipitation to El Nino Warming (W/m**2/K)
Observation
NASA NSIPP-1
NCAR CAM1
UKMO HadAM3
NCAR CAM2
GFDL AM2p10
NCAR CAM3
GFDL AM2p12
a
b
c
d
e
f
g
h
30N 25N 20N 15N 10N 5N EQ 5S 10S 15S 20S 25S 30S
120E 140E 160E 180 160W 140W 120W 100W 80W
-180 -150 -120 -90 -60 -30 30 60 90 120 150 180

Fig.5

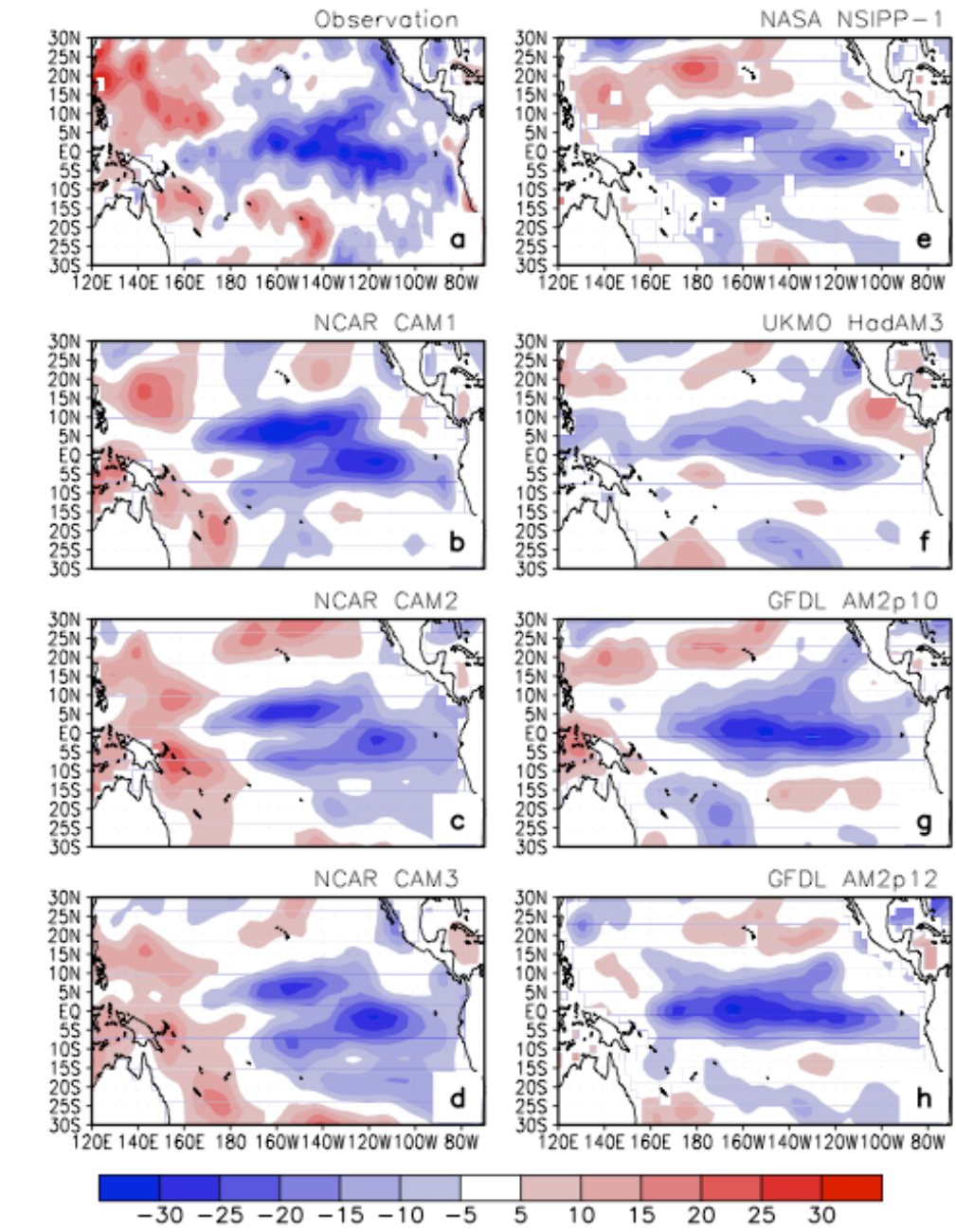
Spatial pattern of response of Da to El Nino Warming (W/m**2/K)
Observation
NASA NSIPP-1
NCAR CAM1
UKMO HadAM3
NCAR CAM2
GFDL AM2p10
NCAR CAM3
GFDL AM2p12
a
b
c
d
e
f
g
h
30N 25N 20N 15N 10N 5N EQ 5S 10S 15S 20S 25S 30S
120E 140E 160E 180 160W 140W 120W 100W 80W
-30 -25 -20 -15 -10 -5 5 10 15 20 25 30

Fig.6

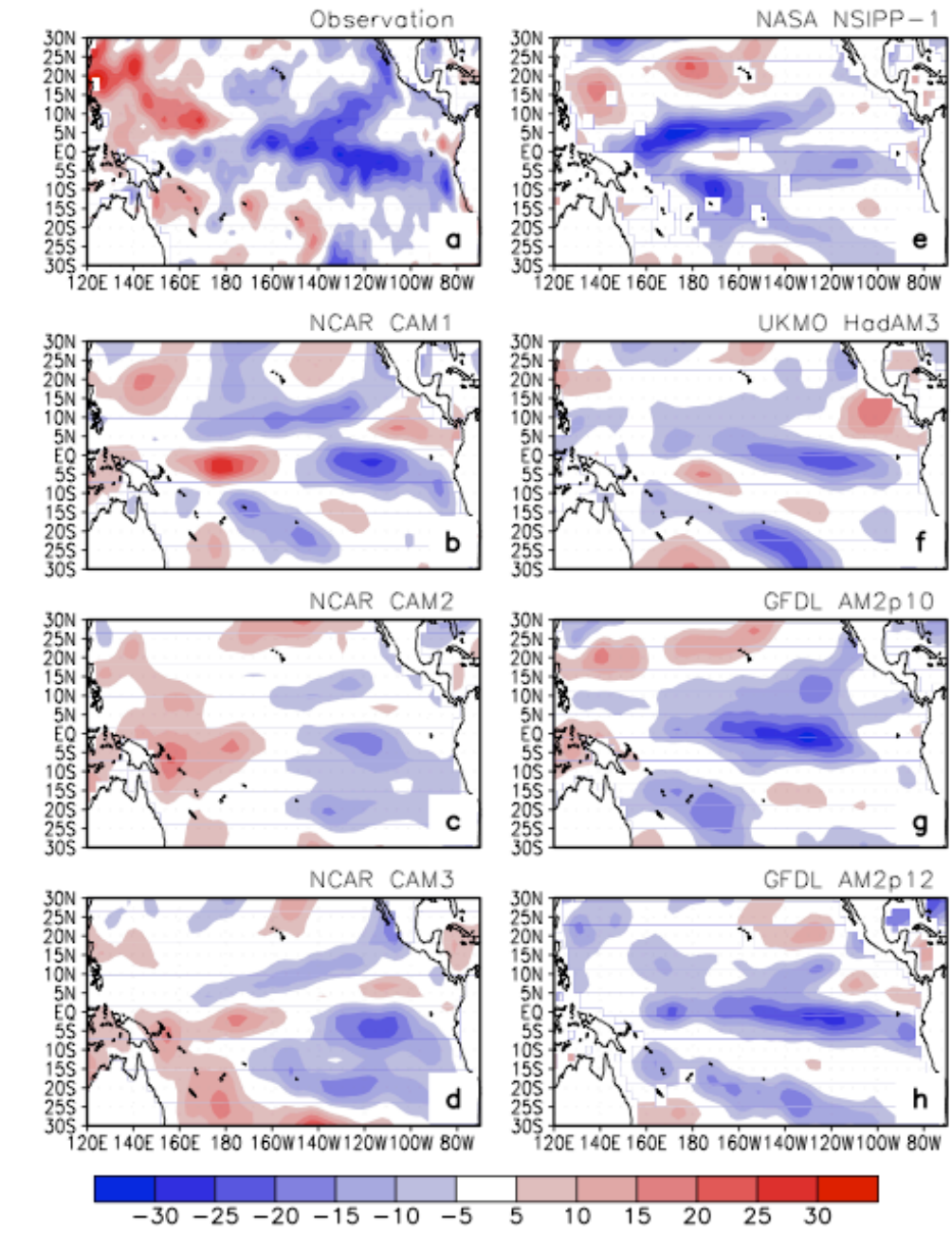
Spatial pattern of response of Fs to El Nino Warming (W/m**2/K)
Observation
NASA NSIPP-1
NCAR CAM1
UKMO HadAM3
NCAR CAM2
GFDL AM2p10
NCAR CAM3
GFDL AM2p12
a
b
c
d
e
f
g
h
30N 25N 20N 15N 10N 5N EQ 5S 10S 15S 20S 25S 30S
120E 140E 160E 180 160W 140W 120W 100W 80W
−30 −25 −20 −15 −10 −5 5 10 15 20 25 30

Fig.7